Automatic ROI Size Selection and Parameter Initialization for Model-Based Localization of 3D Anatomical Point Landmarks

Stefan Wörz and Karl Rohr

School of Information Technology, Computer Vision & Graphics Group
International University in Germany, 76646 Bruchsal
Email: {woerz,rohr}@i-u.de

Abstract. We introduce a new approach for the automatic selection of an optimal 3D ROI size for effective fitting of a deformable model for the purpose of landmark localization. In addition, we propose an algorithm to initialize the parameters of our previously introduced 3D ellipsoidal intensity model. The newly developed approaches have been successfully applied to 3D synthetic data as well as 3D MR images.

1 Introduction

Landmarks are important image features for the registration of 3D medical images. There exist two main approaches for the automated localization of 3D anatomical point landmarks: one based on 3D differential operators (e.g., [1,2]) and the other based on deformable models (e.g., [3]). While being computationally efficient, differential operators are relatively sensitive to noise, which leads to false detections and also affects the localization accuracy. On the other hand, approaches based on deformable models generally exploit contour information of the anatomical structures. In [3], we described an approach based on parametric *intensity* models. We considered tip-like anatomical structures and introduced an ellipsoidal intensity model for landmark localization.

Model-based approaches for landmark localization need to choose a suitable size of the region-of-interest (ROI). The ROI should be large enough to capture enough image information to guarantee a successful localization of the landmark. On the other hand, if the ROI is too large it might contain neighboring structures which negatively influence the accuracy. In addition, for the fitting process we also need starting values for the model parameters. An improper initialization can lead to inaccurate localizations or false fitting results. Often, the ROI size as well as the model parameters are initialized manually. Work on automatic 3D ROI size selection can hardly be found. In [4], an approach is presented based on the statistical uncertainty of a differential edge intersection approach. This approach has been designed for ideally sharp tip-like landmarks, which is an improper approximation of tip-like structures which are typically rounded.

Fig. 1. Sketch of a (half-) ellipse with several image gradients and the resulting dominant gradient direction highlighted (left) as well as with a neighboring structure (hatched ellipse) and two different ROIs (center). The right sketch shows the surface normal, the principal directions, and the principal curvatures at the tip of an ellipsoid.
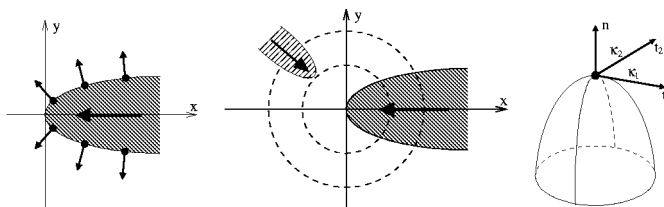
We have developed a new approach for the selection of an optimal 3D ROI size for effective fitting of a deformable model. We exploit the dominant direction of the image gradient in the neighborhood of the landmark position. In comparison to the statistical uncertainty approach [4], the new approach 1) can cope with rounded tip-like structures of ellipsoidal shape, 2) detects more effectively and accurately the optimal ROI size in the presence of typical neighboring structures (e.g., sulci close to the tips of the ventricular system), 3) is more robust against image noise as well as variations of the initial position, and 4) is much simpler and computationally less expensive. In addition, we developed an algorithm to initialize the parameters of our 3D ellipsoidal intensity model [3].

2 ROI Size Selection

To select an optimal ROI size we determine the dominant gradient $\mathbf{d}_r$ of a spherical 3D ROI of radius r. The dominant gradient is obtained by computing the sum of the image gradients at all voxels within the ROI, i.e. $\mathbf{d}_r = \sum_{\mathbf{x} \in \mathrm{ROI}} \nabla g\,(\mathbf{x})$. The main contribution to $\mathbf{d}_r$ typically results from the boundary of the anatomical structure itself and potential neighboring structures whereas homogenous regions have only a small influence. For an isolated rounded tip-like structure similar to a (half-) ellipsoid, summing up the image gradients results in a dominant gradient pointing along the center line of the ellipsoid (see Fig. 1). The reason is that the components of the image gradients pointing perpendicular to the center line compensate each other over the boundary of the ellipsoid, while only the components pointing along the center line contribute to the dominant gradient. When a neighboring structure is additionally captured within the ROI, then the direction of the dominant gradient is generally changed. In our approach we exploit this observation. In order to select an optimal ROI size, we compare for increasing radii r the direction of the dominant gradient $\mathbf{d}_{r-1}$ of a spherical ROI with the direction of the dominant gradient of an adjacent spherical shell (thickness of 1 voxel). The dominant gradient of the spherical shell is given by $\mathbf{d}_r - \mathbf{d}_{r-1}$. As a measure for the change of the direction, we compute the angle δ_r between both dominant gradients $\mathbf{d}_{r-1}$ and $\mathbf{d}_r - \mathbf{d}_{r-1}$, which is given by

$$\delta_r = \arccos\left(\left\langle \frac{\mathbf{d}_{r-1}}{\|\mathbf{d}_{r-1}\|}, \frac{\mathbf{d}_r - \mathbf{d}_{r-1}}{\|\mathbf{d}_r - \mathbf{d}_{r-1}\|} \right\rangle\right) \tag{1}$$

Table 1. Results of estimating the optimal ROI size in synthetic images for the statistical uncertainty approach and the new approach for different neighboring structures. The proportions of correct estimates within 1 and 2 voxels accuracy are given.

Distances: 5-14 voxel	Accuracy [voxel]	Sphere	Ellipsoid 0°	Ellipsoid 45°	Ellipsoid 90°	Average
Statistical uncertainty approach	±1	25.5%	15.8%	1.6%	0.1%	10.8%
	±2	48.6%	16.0%	5.3%	17.9%	22.0%
Dominant gradient approach	±1	84.7%	83.1%	84.2%	86.3%	84.6%
	±2	96.3%	91.7%	95.1%	97.8%	95.2%

where $\langle \cdot, \cdot \rangle$ denotes the inner product. The optimal ROI size is determined by the largest ROI before a significant change of δ_r occurs. A significant change is detected when δ_r exceeds a threshold T (in our case we chose $T = 22.5°$) or when δ_r has maximal increase before a local maximum of $T/2 \leq \delta_{lmax} < T$.

3 Parameter Initialization of the Ellipsoidal Model

For the automatic initialization of the 16 parameters of our ellipsoidal intensity model (3D position and orientation, semi-axes, intensity levels, image smoothing, tapering, and bending), we propose the following strategy. For a given coarse position of the landmark, first the optimal ROI size is determined automatically (see Sect. 2). Within this ROI for landmark detection, the 3D differential operator $Op4 = det\mathbf{C}_g$ is applied [2], where $\mathbf{C}_g$ is the averaged dyadic product of the image gradient. To refine this position we apply the three-step procedure in [5], which results in a sub-voxel position. The position closest to the coarse position with a positive Gaussian curvature (for an isointensity surface) is used as the initial position of the model.

In addition, the image gradient and the principal curvatures κ_1 and κ_2 of the local isointensity surface at this point (see Fig. 1) are computed to determine the initial orientation as well as the size of the three semi-axes (r_x, r_y, r_z). Here, we face the problem that we have three semi-axes but only two relations between the curvatures and the semi-axes: $\kappa_1 = r_z/r_x^2$ and $\kappa_2 = r_z/r_y^2$. In our case we initialize r_z with the radius of the ROI (note, the tip of the ellipsoid w.r.t. r_z is the landmark position). The initial values for the intensity levels of the surrounding tissue and the anatomical structure are determined using the minimal and maximal intensities of the ROI (after median filtering). The initial value for the smoothing parameter is always set to 1 and the remaining model parameters for the global deformations are always set to zero, thus the ellipsoidal model is always initialized as an (undeformed) ellipsoid.

4 Experimental Results: ROI Size Selection

Our approach for selecting an optimal ROI size (Sect. 2) has been applied to 3D synthetic data as well as to 3D MR images of the human head. We generated in total 5600 different 3D synthetic images. Each image contains a tip-like structure of varying orientation and size (generated by our ellipsoidal model) and a

neighboring structure in a varying distance and orientation (either a smoothed thin ellipsoid or sphere) as well as added Gaussian noise ($\sigma_n = 3$ grey levels). We simulated neighboring structures at distances between 5 and 14 voxels and, in case of the thin ellipsoid, at different angles of $0°$, $45°$, and $90°$. The contrast for both the ellipsoid and the neighboring structure was 100 grey levels. Since the distances are between 5 and 14 voxels, the optimal ROI radii are also between 5 and 14 voxels. From the experiments we found that the new approach is quite robust against noise and successfully estimates the optimal ROI size: for ca. 85% of the images, the correct ROI size has been detected within 1 voxel accuracy. For a comparison we also applied the statistical uncertainty approach [4], which yielded only ca. 11% (see Table 1). We also applied our approach to real 3D MR images of the human head (see Sect. 5) and obtained quite good results.

5   Experimental Results: Parameter Initialization

Our approach for automatic parameter initialization of the ellipsoidal intensity model has been applied to 3D synthetic data as well as to two 3D MR images of the human head. In the synthetic experiments we applied model fitting using automatic parameter initialization (including the selection of the ROI size) given 3D image data generated by the model itself with added Gaussian noise. For 1000 experiments with different parameter settings but without global deformations, model fitting succeeded in 99.5% of the cases with an average localization error of 0.12 voxels. In comparison, the 3D differential operator Op4 in conjunction with the three-step refinement yielded an average error of 1.65 voxels. For 1000 similar experiments including global deformations, automatic initialization with subsequent model fitting succeeded in 99.2% of the cases with an average localization error of 0.33 voxels. In comparison, the refined 3D differential operator Op4 yielded 1.64 voxels.

In addition, we applied our approach to two 3D MR images (data sets C06 and Woho). Table 2 shows the fitting results for the tips of six ventricular horns (left and right frontal, occipital, and temporal horns). Note, model fitting was not successful for the right frontal and the left temporal horn in the C06 data set (because of a relatively poor estimate of the initial orientation and position) and for both occipital horns in the Woho data set (the reason is a rather untypical anatomical structure). For the remaining 8 landmarks it turned out that the automatic initialization is quite reliable and allows quite good fitting results. The average distance between the estimated landmark positions and ground truth positions computes to $\bar{e} = 1.63mm$. In comparison, using the refined 3D differential operator Op4, we obtain an average distance of $\bar{e}_{Op4, refine} = 2.33mm$. Fitting results are visualized in Fig. 2 using 3D Slicer (SPL, Boston).

6   Discussion

The experiments verify the applicability of our new approach, which estimates an optimal ROI size such that neighboring structures are not captured. In combination with the initialization of the parameters of our ellipsoidal model this allows a fully automated localization of landmarks.

Table 2. Fitting results for the ventricular horns in two 3D MR images (C06 and Woho). The selected radius r of the ROI, the estimated landmark position, intensity levels, and the distance e to the ground truth position are given. For comparison, the distance of the refined differential operator Op4 to the ground truth position is listed.

	r	$\hat{x}_0$	$\hat{y}_0$	$\hat{z}_0$	$\hat{a}_0$	$\hat{a}_1$	e	$e_{Op4,\,refine}$
Left frontal horn	9	149.44	78.58	70.16	92.6	19.6	1.52mm	2.97mm
Left occipital horn	6	144.30	200.79	52.53	84.6	15.6	0.65mm	3.21mm
Right occipital horn	6	107.33	195.92	57.00	87.3	19.8	1.23mm	1.73mm
Right temporal horn	7	98.79	112.15	40.59	79.7	20.2	0.84mm	1.83mm
Left frontal horn	8	111.27	78.22	101.83	126.3	21.8	2.25mm	1.98mm
Right frontal horn	9	111.50	75.45	131.20	126.3	23.8	2.61mm	1.93mm
Left temporal horn	6	136.45	111.59	89.59	115.1	18.2	2.18mm	1.25mm
Right temporal horn	6	130.48	113.52	147.38	110.8	26.1	1.76mm	3.74mm
						Mean	1.63mm	2.33mm

Fig. 2. Fitted ellipsoidal model for the left and right frontal ventricular horn within the MR image Woho (left) and the left (center) and right occipital horn (right) within the MR image C06. The marked axes indicate the estimated landmark positions.
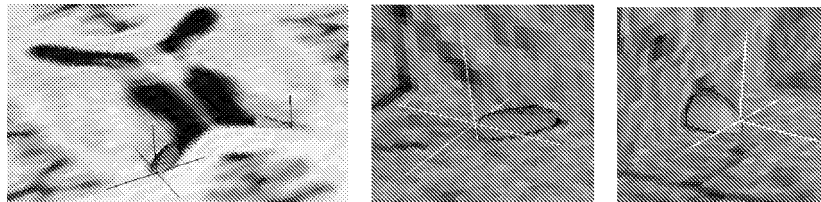
7   Acknowledgement

References

1. J.-P. Thirion, "New Feature Points based on Geometric Invariants for 3D Image Registration", *Int. J. of Computer Vision* 18:2, 1996, 121–137
2. K. Rohr, "On 3D differential operators for detecting point landmarks", *Image and Vision Computing* 15:3, 1997, 219–233
3. S. Wörz and K. Rohr, "Localization of Anatomical Point Landmarks in 3D Medical Images by Fitting 3D Parametric Intensity Models", *Proc. IPMI'03*, Ambleside, UK, July 20-25, 2003, *LNCS* 2732, Springer-Verlag Berlin Heidelberg, 2003, 76–88
4. S. Frantz, K. Rohr, and H.S. Stiehl, "Improving the Detection Performance in Semi-automatic Landmark Extraction", *Proc. MICCAI'99*, Cambridge, UK, Sep. 19-22, 1999, *LNCS* 1679, Springer-Verlag Berlin Heidelberg, 1999, 253–262
5. S. Frantz, K. Rohr, and H.S. Stiehl, "Multi-Step Differential Approaches for the Localization of 3D Point Landmarks in Medical Images", *J. of Computing and Information Technology (CIT)*, 6:4, 1998, 435–447